AUTHOR(S):

Nguyen, Dinh Thi; Le, Thuong Manh; Hattori, Tsuyoshi; Takarada-Iemata, Mika; Ishii, Hiroshi; Roboon, Jureepon; Tamatani, Takashi; ... Saito, Shunsuke; Mori, Kazutoshi; Hori, Osamu

京都大学学術情報リポジトリ
KURENAI 紅
Kyoto University Research Information Repository

KURENAI 紅
京都大学学術情報リポジトリ
Kyoto University Research Information Repository

scientific reports

Check for updates

OPEN

The ATF6β-calreticulin axis promotes neuronal survival under endoplasmic reticulum stress and excitotoxicity

Dinh Thi Nguyen[1], Thuong Manh Le[1,7], Tsuyoshi Hattori[1], Mika Takarada-Iemata[1], Hiroshi Ishii[1], Jureepon Roboon[1], Takashi Tamatani[1], Takayuki Kannon[2], Kazuyoshi Hosomichi[2], Atsushi Tajima[2], Shusuke Taniuchi[3], Masato Miyake[3], Seiichi Oyadomari[3], Takashi Tanaka[4], Nobuo Kato[5], Shunsuke Saito[6], Kazutoshi Mori[6] & Osamu Hori[1✉]

While ATF6α plays a central role in the endoplasmic reticulum (ER) stress response, the function of its paralogue ATF6β remains elusive, especially in the central nervous system (CNS). Here, we demonstrate that ATF6β is highly expressed in the hippocampus of the brain, and specifically regulates the expression of calreticulin (CRT), a molecular chaperone in the ER with a high Ca^{2+}-binding capacity. CRT expression was reduced to ~ 50% in the CNS of $Atf6b^{-/-}$ mice under both normal and ER stress conditions. Analysis using cultured hippocampal neurons revealed that ATF6β deficiency reduced Ca^{2+} stores in the ER and enhanced ER stress-induced death. The higher levels of death in $Atf6b^{-/-}$ neurons were recovered by ATF6β and CRT overexpressions, or by treatment with Ca^{2+}-modulating reagents such as BAPTA-AM and 2-APB, and with an ER stress inhibitor salubrinal. In vivo, kainate-induced neuronal death was enhanced in the hippocampi of $Atf6b^{-/-}$ and $Calr^{+/-}$ mice, and restored by administration of 2-APB and salubrinal. These results suggest that the ATF6β-CRT axis promotes neuronal survival under ER stress and excitotoxity by improving intracellular Ca^{2+} homeostasis.

The endoplasmic reticulum (ER) is an intracellular organelle in which secretory proteins and lipids are synthesized, and intracellular Ca^{2+} is stored. However, recent studies demonstrated that a stress response occurs in the ER. When cells are exposed to specific conditions such as impaired Ca^{2+} homeostasis, energy shortage, and increased protein synthesis, unfolded proteins accumulate in the ER, leading to a condition generally termed ER stress[1]. In the central nervous system (CNS), pathological situations such as brain ischemia, neurodegeneration, excitotoxicity and demyelination are tightly associated with ER stress[2–4]. Cells can respond to ER stress by activating the unfolded protein response (UPR). There are at least three transducers of the UPR, namely, protein kinase R (PKR)-like ER kinase (PERK), inositol-requiring enzyme 1 (IRE1), and activating transcription factor 6 (ATF6)[5,6]. Among these, ATF6 is responsible for induction of the major molecular chaperones in the ER, such as glucose-regulated protein 78 (GRP78) and glucose-regulated protein 94 (GRP94), in addition to several ER-associated degradation components such as homocysteine-responsive ER-resident ubiquitin-like domain member 1 protein and ER degradation enhancing α mannosidase[5,7]. In mammals, there are two subtypes of ATF6, called ATF6α and ATF6β. Both molecules are type II transmembrane proteins in the ER and translocate to the Golgi apparatus for cleavage upon ER stress. Although ATF6α plays a dominant role in the transcriptional activation

[1]Department of Neuroanatomy, Graduate School of Medical Sciences, Kanazawa University, 13-1 Takara-Machi, Kanazawa City, Ishikawa 920-8640, Japan. [2]Department of Bioinformatics and Genomics, Graduate School of Advanced Preventive Medical Sciences, Kanazawa University, Kanazawa, Japan. [3]Division of Molecular Biology, Institute for Genome Research, Institute of Advanced Medical Sciences, Tokushima University, Tokushima, Japan. [4]Department of Anatomy II, Kanazawa Medical University, Kahoku, Japan. [5]Department of Physiology I, Kanazawa Medical University, Kahoku, Japan. [6]Department of Biophysics, Graduate School of Science, Kyoto University, Kyoto, Japan. [7]Present address: Department of Human Anatomy, Hanoi Medical University, Hanoi, Vietnam. ✉email: osamuh3@staff.kanazawa-u.ac.jp

nature portfolio   1

in response to ER stress, ATF6α/β-mediated adjustment of chaperone levels to meet the increased demands in the ER is essential for the development of the notochord[7,8].

We previously reported that ATF6α contributes to both neuronal survival and glial activation in different neuropathological situations. Deletion of ATF6α or that of a downstream molecular chaperone, glucose-regulated protein 170 (GRP170)/Oxygen-regulated protein150 (ORP150), sensitizes hippocampal neurons to glutamate-induced toxicity most likely via Ca^{2+} overload and neuronal hyperactivity in vivo[9,10]. *Atf6α* deficiency is also associated with reduced astroglial activation and glial scar formation in mouse models of Parkinson's disease[11] and stroke[12], respectively, both of which are associated with an enhanced level of neuronal death. By contrast, in experimental autoimmune encephalomyelitis mice, a model of multiple sclerosis, and cultured microglia, *Atf6α* deficiency suppresses microglial activation, clinical symptoms and demyelination via a mechanism involving rapid degradation of NF-κB p65 by the proteasome[13].

In contrast with the role of ATF6α in the ER stress response/UPR and ER stress-related pathophysiologies, the function of ATF6β is largely unknown, especially in the CNS. Transcriptional activity of ATF6β is reportedly much weaker than that of ATF6α[14]. However, recent reports demonstrated that ATF6α and ATF6β may have overlapping and differential functions in the mouse heart[15,16]. We therefore sought to investigate the expression and possible roles of ATF6β in the CNS under normal and ER stress conditions. Here, we demonstrate that calreticulin (CRT), a molecular chaperone in the ER with a high Ca^{2+}-binding capacity, is a unique target of ATF6β in the CNS, and the ATF6β-CRT axis plays a critical role for the neuronal survival under ER stress and excitotoxity by improving intracellular Ca^{2+} homeostasis.

Results

Expression of ATF6β in the CNS and other tissues.   We first verified the tissue distribution of ATF6β in mice. Quantitative real-time PCR (qRT-PCR) revealed that *Atf6b* mRNA was broadly expressed, but was most highly expressed in the hippocampus of the brain among the tissues analyzed (Fig. 1A). Further analysis of cultured cells revealed that expression of *Atf6b* mRNA was higher in hippocampal neurons than in cortical neurons and astrocytes under normal conditions (Fig. 1B). Consistently, in situ hybridization revealed that *Atf6b* mRNA was highly expressed in hippocampal neurons (Fig. 1C). These patterns were in contrast with those of *Atf6a* mRNA, which was more ubiquitously expressed (Fig. S1A,B). There was no significant difference in *Atf6b* mRNA levels between male and female mice (Fig. S1C).

We next analyzed expression of *Atf6b* mRNA under ER stress. Treatment of cultured hippocampal neurons with the ER stressors tunicamycin (Tm) and thapsigargin (Tg) significantly increased expression of *Atf6b* mRNA (1.5 to twofold increase) (Fig. 1D), although these increases were smaller than those in expression of *Atf6a* mRNA (5–6.5-fold increase) (Fig. S1D). At the protein level, both the full-length 110 kDa protein (FL) and a cleaved N-terminal 60 kDa fragment (NTF) of ATF6β were detected in primary hippocampal neurons. The level of this fragment was low under normal conditions, but increased as early as 2 h after Tg treatment or 1 h after dithiothreitol (DTT) treatment, the latter another ER stressor (Fig. 1E). These results suggest that ATF6β functions in neurons especially under ER stress.

Calr is a unique target gene of ATF6β in the CNS.   To identify downstream molecules of ATF6β in the CNS, RNA-sequencing was performed using hippocampal brain samples from wild-type (WT) and *Atf6b*$^{-/-}$ mice. A total of 55,531 genes were examined. We filtered genes in two ways. When filtering genes stringently with FPKM values in WT mice higher than 10 and q values smaller than 0.05, only 2 downregulated genes and 4 upregulated genes were identified in *Atf6b*$^{-/-}$ mice (Table 1). Although expression of *Atf6b* mRNA was observed to some extent in *Atf6b*$^{-/-}$ mice, this may be due to the presence of the 5' *Atf6b* transcript with exon 1–9 in these mice, as exon 10 and 11 were deleted by homologous recombination[7] (Fig. S2). Besides *Atf6b*, only *Calr*, which encodes CRT, a molecular chaperone in the ER with a high Ca^{2+}-binding capacity, was downregulated in *Atf6b*$^{-/-}$ mice (Table 1). By contrast, in case filtering genes less stringently with FPKM values in WT mice higher than 10 and p values smaller than 0.05, 22 downregulated genes and 27 upregulated genes were identified in *Atf6b*$^{-/-}$ mice (Table S1). *Calr* was again identified as a gene downregulated in *Atf6b*$^{-/-}$ mice, and interestingly, six ER stress-responsive genes, namely, *Hpsa5* (GRP78), *Pdia4* (ERP72), *Dnajb11*, *Atf4*, *Wfs1*, and *P4ha1* were upregulated in *Atf6b*$^{-/-}$ mice (Table S1 right columns). These results suggest that *Atf6b* deficiency may cause mild ER stress in the brain under normal conditions. RNA-sequencing also indicated that expression level of *Calr* was highest among the major molecular chaperones in the ER in WT brains (Table S2). Taken together with previous reports demonstrating possible roles of ATF6β in the expression of molecular chaperones in the ER[7,8,16], we decided to focus on ATF6β-CRT axis in further experiments.

Consistent with the RNA-sequencing data, RT-qPCR using hippocampi of WT, *Atf6a*$^{-/-}$, and *Atf6b*$^{-/-}$ mice revealed that expression of *Calr* mRNA was reduced to ∼50% in *Atf6b*$^{-/-}$ brains, but not in *Atf6a*$^{-/-}$ brains (Fig. S3A). This was in contrast with expression of *Hspa5* (GRP78) mRNA, which was reduced in *Atf6a*$^{-/-}$ brains, but increased in *Atf6b*$^{-/-}$ brains (Fig. S3A). Similar differences in expression of *Hsp90b1* (GRP94) mRNA were observed, although these were not significant. Expression of *Canx*, which encodes calnexin, another molecular chaperone in the ER with similarities to CRT, was unaffected by *Atf6a* and *Atf6b* deficiency (Fig. S3A).

The effect of *Atf6b* deletion on CRT expression was next analyzed in different tissues under normal conditions (Fig. 2A,B). Both qRT-PCR (Fig. 2A) and western blotting (Fig. 2B) revealed that CRT expression was significantly lower in the CNS, but not in other tissues tested, in *Atf6b*$^{-/-}$ mice than in WT mice.

Effect of ATF6β deletion on CRT promoter activity.   To analyze the role of ATF6β in CRT expression at the promoter level, reporter assays were performed with chloramphenicol acetyltransferase (CAT) plasmids containing 1763 bp (pCC1), 415 bp (pCC3), and 115 bp (pCC5) of the mouse CRT promoters[17], and luciferase
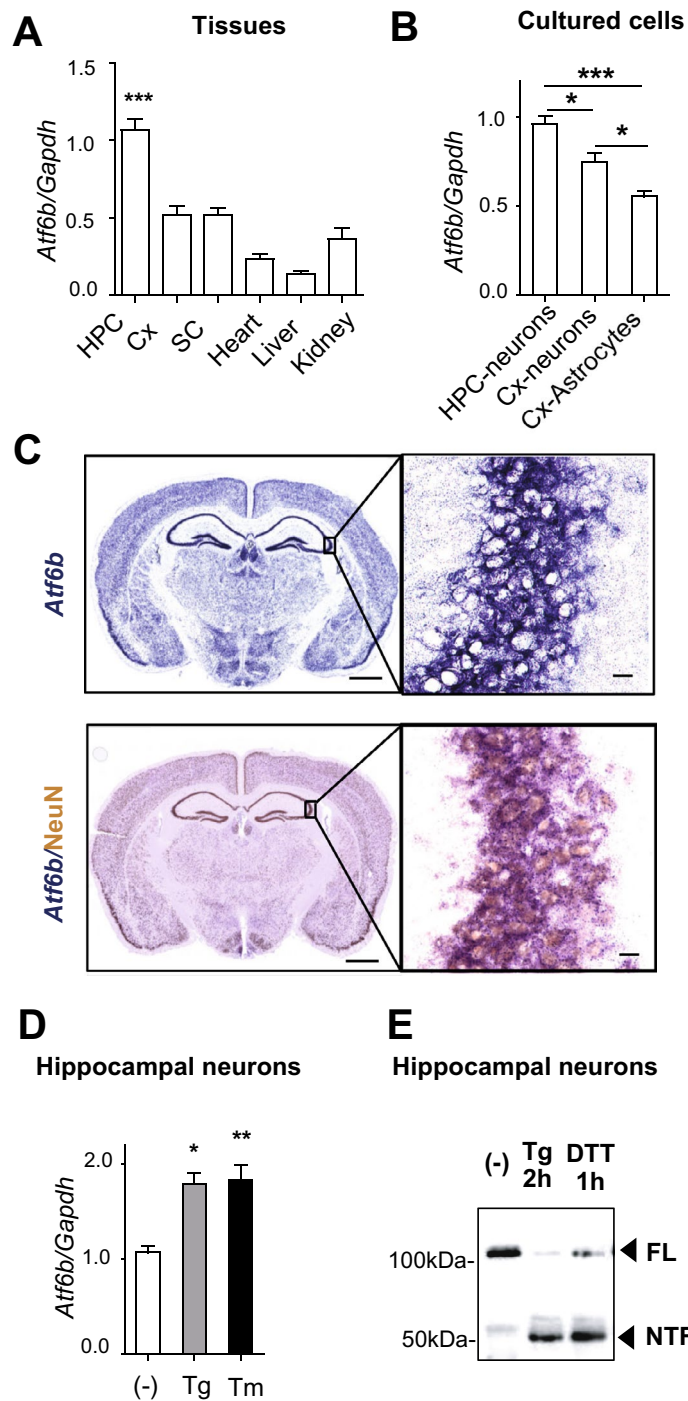
Figure 1. Expression and activity of ATF6β. (**A,B**) Expression of *Atf6b* mRNA in normal tissues (n = 5 mice) (**A**) and in cultured cells (n = 3–8) (**B**). HPC: hippocampus, *Cx* cerebral cortex, *SC* spinal cord. Total RNA was isolated from the indicated samples and qRT-PCR was performed. Data are shown as mean ± SEM. *p < 0.05, ***p < 0.001 by a one-way ANOVA followed by the Tukey test. (**C**) In situ hybridization (upper panel) and in situ hybridization-immunohistochemistry (lower panel) of *Atf6b* mRNA in the normal brain. Images in the right panels are enlarged views of the CA3 area. Scale bars: 200 μm (left panels) and 25 μm (right panels). Typical images from three independent experiments are shown. (**D**) qRT-PCR analysis of expression of *Atf6b* mRNA in primary hippocampal neurons under ER stress. Cells were treated with Tg (300 nM) or Tm (1 μg/ml) for 8 h and then qRT-PCR was performed. n = 3. Data are shown as mean ± SEM. *p < 0.05, **p < 0.01 by a one-way ANOVA followed by the Tukey test. (**E**) Activation of ATF6β by ER stress in primary hippocampal neurons. Cells were treated with Tg (300 nM) for 2 h or DTT for 1 h. Extracted proteins were subjected to western blotting. The typical data from two independent experiments are shown. *FL* full length, *NTF* N-terminal fragment.

3

Downregulated genes in *Atf6b*$^{-/-}$ brain					Upregulated genes in *Atf6b*$^{-/-}$ brain				
Gene	WT	*Atf6b*$^{-/-}$	log2 (fold-change)	q-value	*Gene*	WT	*Atf6b*$^{-/-}$	log2 (fold-change)	q-value
Atf6b	31.633	7.66511	-2.04505	<0.0465921	*Gm47283*	13.354	43.6105	1.70741	<0.0465921
Calr	203.013	123.236	-0.720147	<0.0465921	*Igf2*	19.0054	39.9251	1.07089	<0.0465921
					Ptgds	452.8	942.637	1.05783	<0.0465921
					Mgp	20.9161	35.9567	0.781646	<0.0465921

Table 1. Differentially expressed genes in *Atf6b*$^{-/-}$ brain (q < 0.05). Pink and blue colors indicate Upregulated-genes and downregulated-genes in *Atf6b*$^{-/-}$ brains.

plasmids containing 459 bp of the WT (huCRT(wt)) and mutant (huCRT(mut)) human CRT promoters, with the latter containing mutated sequences of two ER stress-responsive elements (ERSEs)[18] (Fig. 2C). Upon transfection of pCC1 or pCC3, promoter activity was lower in *Atf6b*$^{-/-}$ hippocampal neurons (59% in pCC1 and 58% in pCC3, respectively) than in WT hippocampal neurons (Fig. 2D upper graph). Overexpression of ATF6β cDNA restored the promoter activity in *Atf6b*$^{-/-}$ neurons (103% in pCC1 and 105% in pCC3). Similarly, upon transfection of huCRT(wt), CRT promoter activity was lower (59%) in *Atf6b*$^{-/-}$ neurons than in WT neurons, and overexpression of ATF6β cDNA restored promoter activity to 87% in *Atf6b*$^{-/-}$ neurons (Fig. 2D lower graph). By contrast, upon transfection of pCC5 (Fig. 2D upper graph) or huCRT(mut) (Fig. 2D lower graph), CRT promoter activity was much lower in either WT or *Atf6b*$^{-/-}$ neurons and was not restored at all by overexpression of ATF6β cDNA, suggesting that ERSEs are essential for ATF6β-mediated CRT promoter activation. The effect of the active and dominant-negative forms of ATF6β cDNAs on the CRT promoter activity was also analyzed by overexpressing ATF6β(392) and ATF6β(392)ΔAD cDNAs, respectively, in WT and *Atf6b*$^{-/-}$ hippocampal neurons (Fig. 2E). As expected, ATF6β(392) strongly restored the promoter activity in *Atf6b*$^{-/-}$ neurons (175%), while ATF6β(392)ΔAD had no effect (Fig. 2F). Furthermore, ATF6β(392)ΔAD reduced the promoter activity of WT neurons to the level similar to that of *Atf6b*$^{-/-}$ neurons (Fig. 2F).

Similar results were obtained in mouse embryonic fibroblasts (MEFs) transfected with pCC1, huCRT(wt), or huCRT(mut) (Fig. S3B). In contrast to CRT promoter activity, GRP78 promoter activity, which was measured using a luciferase plasmid containing 132 bp of the human GRP78 promoter[18], did not differ between WT and *Atf6b*$^{-/-}$ neurons under both normal and ER stress conditions (Fig. S3C).

Effect of ATF6β deletion on expression of molecular chaperones in the ER in primary hippocampal neurons. The effect of ATF6β deletion on the expression of molecular chaperones in the ER was next examined under normal and ER stress conditions using WT and *Atf6b*$^{-/-}$ hippocampal neurons. Consistent with the results obtained using mouse tissues under normal conditions, RT-qPCR revealed that *Calr* expression was significantly lower in *Atf6b*$^{-/-}$ neurons than in WT neurons under both control and ER stress conditions, with the latter induced by Tg (Fig. 3A upper row) and Tm (Fig. 3B lower row). By contrast, expression of other molecular chaperones in the ER such as *Canx* (calnexin), *Hsp90b1* (GRP94), and *Hspa5* (GRP78) was temporally lower in *Atf6b*$^{-/-}$ neurons than in WT neurons after stimulation with Tg (Fig. 3A upper row) or Tm (Fig. 3A lower row). Similarly, western blot analysis revealed that expression of CRT protein was constitutively lower in *Atf6b*$^{-/-}$ neurons than in WT neurons, while protein expression of other molecular chaperones in the ER was similar in *Atf6b*$^{-/-}$ and WT neurons under both normal and ER stress conditions (Fig. 3B).

Finally, gene-silencing experiments were performed to exclude the possibility that the effect of *Atf6b* deletion on CRT expression was indirect due to the long-term absence of *Atf6b*. Transfection of Neuro 2a cells with two sets of ATF6β-targeting siRNAs (ATF6β-siRNA1 and ATF6β-siRNA2) reduced *Atf6b* expression to 30% and 43% and reduced *Calr* expression to 62% and 66%, but did not affect *Hspa5* (GRP78) expression, compared with that in control-siRNA-transfected cells (Fig. S6A).

Effect of ATF6β deletion on Ca^{2+} homeostasis in primary hippocampal neurons. As CRT is involved in the regulation of the ER Ca^{2+} capacity[19], Ca^{2+} levels in the ER were measured by the green fluorescence-Ca^{2+}-measuring organelle-entrapped protein indicator 1 in the ER (G-CEPIA1er)[20]. Consistent with the reduced level of CRT expression in *Atf6b*$^{-/-}$ neurons, Ca^{2+} levels in the ER were lower in *Atf6b*$^{-/-}$ neurons under both normal and ER stress conditions (Fig. 3C left). By contrast, basal Ca^{2+} levels in the cytosol, which were measured by GFP-based Ca^{2+} calmodulin probe 6f (GCaMP6f)[21], were higher in *Atf6b*$^{-/-}$ neurons (Fig. 3C middle). Ca^{2+} levels in the mitochondria, which were measured by CEPIA2 in the mitochondria (CEPIA2mt)[20], were at similar levels between two genotypes under both normal and ER stress conditions (Fig. 3C right). Because these Ca^{2+} measurements may be methodologically affected by expression levels of Ca^{2+}-indicator proteins,
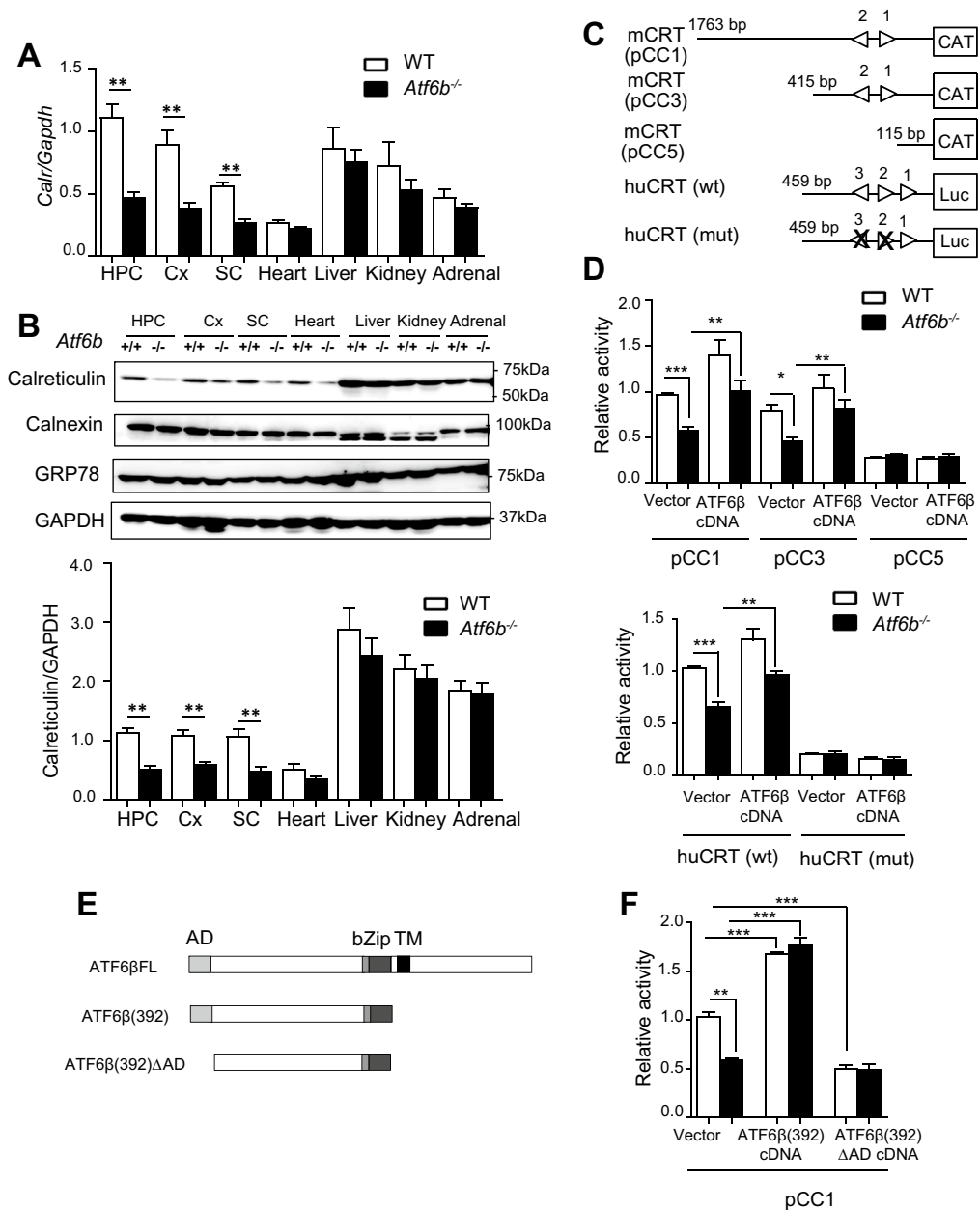
Figure 2. CRT expression in the WT and *Atf6b*−/− mice. (**A**) Expression of *Calr* mRNA in WT and *Atf6b*−/− tissues. Total RNA was isolated from the indicated tissues of each mouse and qRT-PCR was performed. n = 5 mice. Data are shown as mean ± SEM. **p < 0.01 by the Mann–Whitney U test. *HPC* hippocampus, *Cx* cerebral cortex, *SC* spinal cord. (**B**) Expression of CRT protein in WT and *Atf6b*−/− tissues. Protein samples were extracted from the indicated tissues of WT and *Atf6b*−/− mice, and subjected to western blotting. n = 5–7 mice. Data are shown as mean ± SEM. **p < 0.01 by the Mann–Whitney U test. (**C**) Schematic Representation of the promoters used. Triangles indicate the locations and orientations of ERSE motifs that completely or considerably match the consensus CCAATN9CCACG[18]. Numbers indicate nucleotide positions from transcription start site. ERSE2 and ERSE3 of the human CRT promoter were disrupted by mutating their sequences (marked by crosses). (**D**) Reporter assays using cultured hippocampal neurons. The CAT ELISA and luciferase assay were performed using cells transfected with the mouse CRT promoters, pCC1, pCC3, and pCC5 (upper graph), or with the human CRT promoters, huCRT(wt) and huCRT(mt) (lower graph). n = 4. Data are shown as mean ± SEM. *p < 0.05, **p < 0.01, ***p < 0.001, by a two-way ANOVA followed by the Bonferroni test. (**E**) Schematic Representation of the full-length (FL), the active form (392) and the dominant-negative form ((392)ΔAD) of ATF6β[14]. *AD* activation domain, *bZip* the basic leucine zipper domain, *TM* transmembrane domain. (**F**) Reporter assays using cultured WT and *Atf6b*−/− hippocampal neurons. The CAT ELISA assay was performed using cells transfected with the mouse CRT promoter pCC1. n = 3–5 experiments. Data are shown as mean ± SEM. **p < 0.01, ***p < 0.001, by a two-way ANOVA followed by the Bonferroni test.
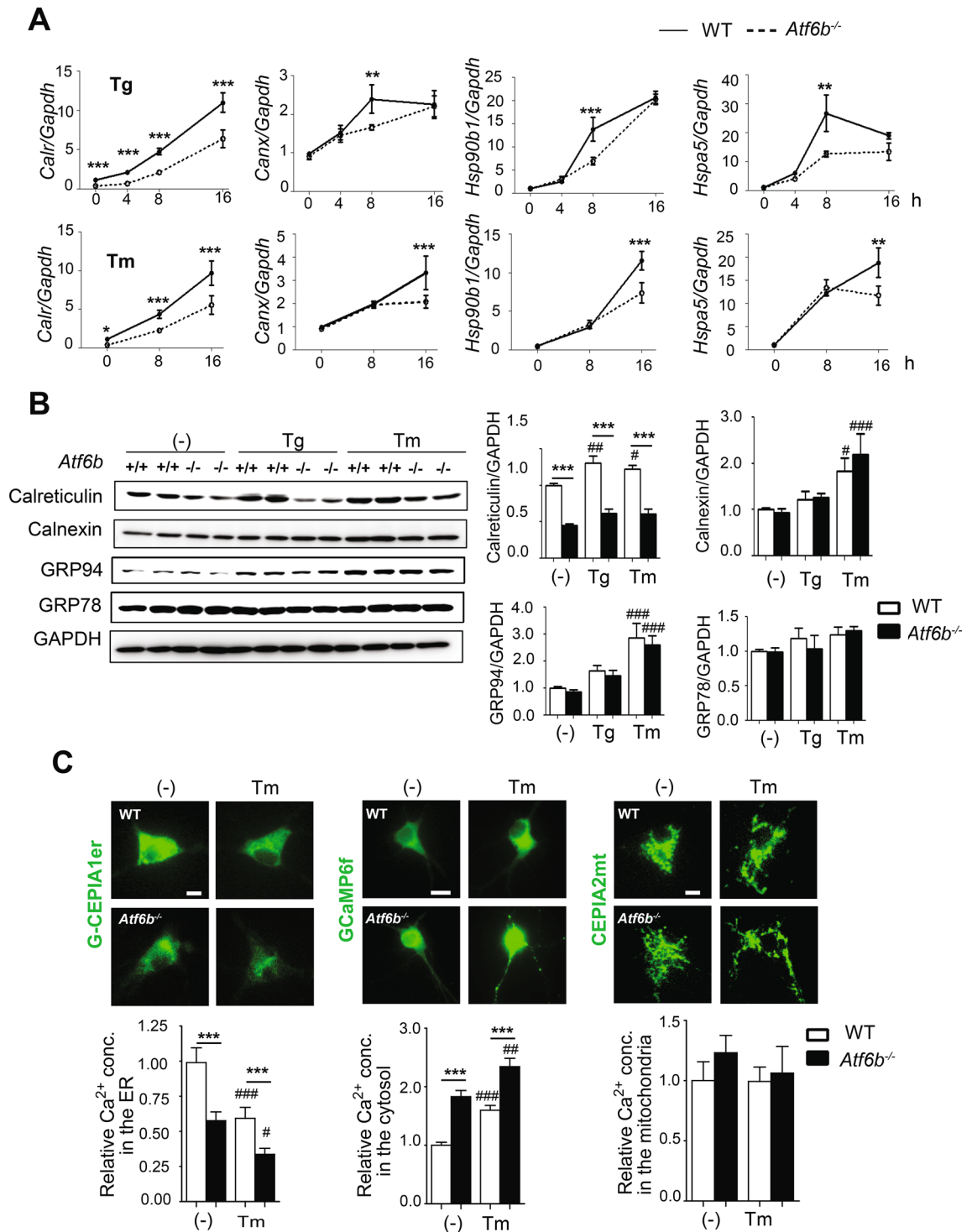
Figure 3. Expression of molecular chaperones in the ER and Ca^{2+} levels in WT and Atf6b$^{-/-}$ hippocampal neurons. (**A**) Total RNA was isolated from WT and Atf6b$^{-/-}$ hippocampal neurons (n = 3–8), and qRT-PCR was performed with the indicated primers. Data are shown as mean ± SEM. *p < 0.05, **p < 0.01, ***p < 0.001 between two genotypes by a two-way ANOVA followed by the Bonferroni test. Note that expression of Calr mRNA was significantly lower in Atf6b$^{-/-}$ neurons than in WT neurons under both normal and ER stress conditions. (**B**) Protein samples extracted from WT and Atf6b$^{-/-}$ hippocampal neurons exposed to control or ER stress conditions for 16 h (n = 5–6) were analyzed by western blotting using antibodies against the indicated proteins. Data are shown as mean ± SEM. ***p < 0.001 between two genotypes and #p < 0.05, ##p < 0.01, ###p < 0.001 compared to normal conditions by a two-way ANOVA followed by the Bonferroni test. Note that expression of CRT protein was significantly lower in Atf6b$^{-/-}$ neurons than in WT neurons under both normal and ER stress conditions. (**C**) Ca^{2+} levels in the ER, cytosol and mitochondria of hippocampal neurons were measured using G-CEPIA1er, GCaMP6f. and CEPIA2mt, respectively under normal and ER stress (Tm for 3 h) conditions. n = 60–250 cells in each condition from two independent experiments. Data are shown as mean ± SEM. ***p < 0.001 between two genotypes and #p < 0.05, ##p < 0.01, ###p < 0.001 compared to normal conditions by a two-way ANOVA followed by the Bonferroni test.

immunocytochemical staining was performed with anti-GFP antibody (Fig. S4) and with anti-Myc antibody (data not shown), the latter antibody recognizes the Myc epitope inserted in G-CEPIA1er and CEPIA2mt. The expression levels of Ca^{2+}-indicator proteins were at similar levels in both genotypes. Furthermore, to see the floor levels of Ca^{2+} in the ER, neurons were treated with Tg for 3 min. G-CEPIA1er-derived, but not CEPIA2mt-derived, fluorescence disappeared in both genotypes (data not shown).

Neuroprotective role of the ATF6β-CRT axis against ER stress-induced neuronal death.

To evaluate whether ATF6β has a neuroprotective role against ER stress, WT and *Atf6b*$^{-/-}$ hippocampal neurons were treated with Tg or Tm and the cell death/survival was evaluated in two ways. Staining of living and dead cells with the fluorescent dyes, calcein-AM (green) and ethidium homodimer-1 (EthD-1, red), respectively, revealed that almost all cells are alive in normal conditions. Treatment with ER stressors induced death and reduced viability of both WT and *Atf6b*$^{-/-}$ neurons, but this effect was more pronounced in *Atf6b*$^{-/-}$ neurons (Fig. 4A). Nuclear localization of EthD-1 was confirmed by the images with single fluorescence for Hoechst 33342 and EthD-1 (Fig. S5). Consistently, immunocytochemical staining using an antibody against the apoptosis marker cleaved caspase-3 (red) and neuronal marker βIII tubulin (green) indicated that activation of caspase-3 and loss of βIII tubulin expression were more prominent in *Atf6b*$^{-/-}$ neurons than in WT neurons under ER stress (Fig. 4B). Similarly, transient silencing of *Atf6b* gene using siRNA enhanced ER stress-induced death of Neuro 2a cells (Fig. S6B,C).

To confirm the neuroprotective role of the ATF6β-CRT axis against ER stress, rescue experiments were performed by transfecting ATF6β and ATF6α cDNAs (Fig. 4C), or by using a lentivirus-mediated CRT overexpression system (LV-CRT) (Fig. 5A,B). When cells were co-transfected with ATF6β and GFP cDNAs, the number of cleaved caspase-3-positive cells in GFP-positive cells was reduced in *Atf6b*$^{-/-}$ neurons. By contrast, the number was not changed in *Atf6b*$^{-/-}$ neurons when cells were co-transfected with ATF6α and GFP cDNAs (Fig. 4C). Consistent with the neuroprotective effect of ATF6β, overexpression of CRT in *Atf6b*$^{-/-}$ neurons restored its expression to a similar level as that in control WT neurons (Fig. 5A), and improved the survival of neurons upon Tm treatment (Fig. 5B).

Similar to the results of *Atf6b*$^{-/-}$ hippocampal neurons, ER stress-induced death was enhanced in *Calr*$^{+/-}$ hippocampal neurons (Fig. 5C).

Effects of Ca²⁺-modulating reagents and an ER stress inhibitor on ER stress-induced neuronal death.

It has been reported that the CRT-mediated Ca^{2+} regulation is critical for modulating neuronal death in a neurodegeneration model[22,23]; therefore, the effects of the Ca^{2+}-modulating reagents O,O′-bis(2-aminophenyl)ethyleneglycol-N,N,N′,N′-tetraacetic acid, tetraacetoxymethyl ester (BAPTA-AM), a cell-permeable Ca^{2+} chelator, and 2-aminophosphate borate (2-APB), an inhibitor of IP3Rs and store-operated channels, and an ER stress inhibitor salubrinal were analyzed in our model. Immunocytochemical analysis revealed that all reagents significantly improved survival of *Atf6b*$^{-/-}$ neurons under ER stress (images are shown in Fig. S7A and quantified data are shown in Fig. 5D). Although it was reported that BAPTA-AM alone caused ER stress and neuronal death at the concentrations higher than 13 μM[24], we confirmed no toxicity of BAPTA-AM and 2-APB at the concentrations used in this study (5 μM and 2 μM, respectively) (Fig. S7B). Furthermore, we analyzed the effect of salubrinal with different concentrations. Significant neuroprotection was observed at 5 and 10 μM, and higher concentration (50 μM or higher) enhanced ER stress-induced neuronal death in our model (Fig. S7C).

Effect of ATF6β deletion on expression of molecular chaperones in the ER after kainate (KA) injection in mice.

Kainate (KA), an agonist of glutamate receptors, causes Ca^{2+}-dependent hyperactivation of neurons, followed by the induction of ER stress and neuronal death in the hippocampus[10]. We and other groups have demonstrated the protective role of UPR signaling in KA-injected mice[2,9,10]. In this study, we investigated the role of ATF6β-CRT axis in these mice. RT-qPCR revealed that expression of *Atf6b*, *Calr*, *Canx*, and *Hspa5* mRNAs mildly, but significantly, increased after injection of KA into the mouse hippocampus (Fig. 6A). Consistent with the results in cultured neurons, the level of *Calr* mRNA, but not of other mRNAs, was reduced to ~50% in *Atf6b*$^{-/-}$ mice under both sham and KA-injected conditions (Fig. 6A). Western blot analysis confirmed that the level of CRT protein was decreased in the *Atf6b*$^{-/-}$ hippocampus under both sham and KA-injected conditions (Fig. 6B).

The neuroprotective role of ATF6β-CRT axis against KA-induced neuronal death.

The neuroprotective effect of ATF6β in vivo was evaluated using KA-injected mice. Consistent with our previous reports[9,10], Nissl staining (Fig. S8A) and immunohistochemical staining for cleaved caspase-3 (Fig. 7A) revealed that KA caused neuronal death in the CA3 region of the hippocampus, which is one of the most KA-sensitive areas. The level of neuronal death was significantly higher in *Atf6b*$^{-/-}$ mice than in WT mice at 1 and 3 days after KA injection (Supplementary Fig. S8A, Fig. 7A). To analyze the involvement of CRT in KA-induced neuronal death, *Calr*$^{+/-}$ mice, which developed normally and showed no gross phenotypes with a reduced level of *Calr* expression (Fig. S8B,C), were injected with KA and neuronal death was evaluated. Consistent with the results obtained with *Atf6b*$^{-/-}$ mice, the level of neuronal death in the hippocampus was significantly higher in *Calr*$^{+/-}$ mice than in WT mice (Fig. 7B).

ATF6β-mediated regulation of neuronal activity and Ca²⁺ homeostasis after KA administration.

To elucidate the mechanism underlying the enhanced level of neuronal death in *Atf6b*$^{-/-}$ hippocampus after KA injection, earlier events following KA injection were investigated. qRT-PCR (Fig. S9A) and immunohistochemistry (Fig. S9B) revealed that expression of the immediate-early genes such as *Fos* (c-Fos), *Fosb*
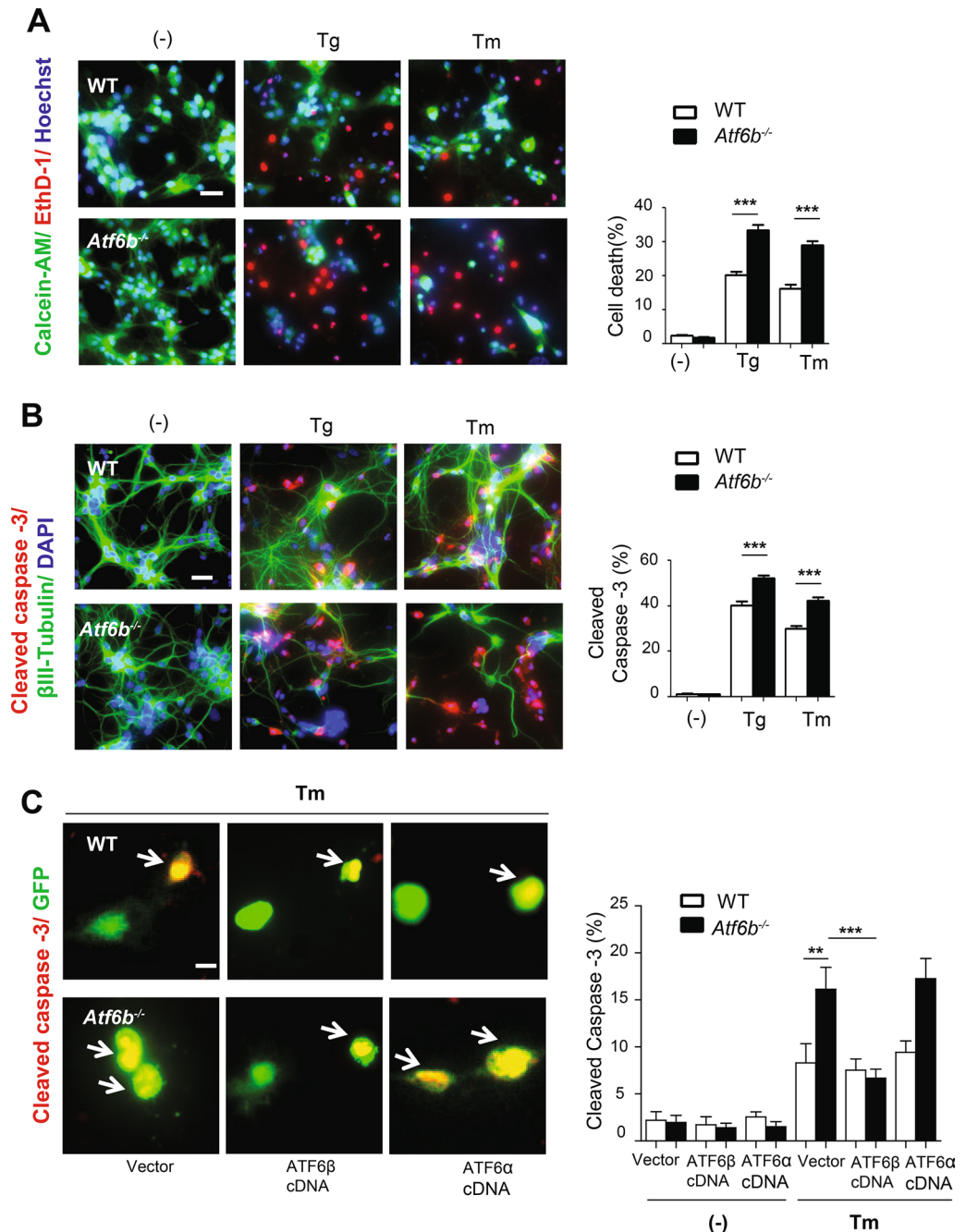
Figure 4. Protection of the primary hippocampal neurons by ATF6β. (**A**) Primary hippocampal neurons were treated with Tg (300 nM) or Tm (1 μg/ml) for 24 h, and cell survival/death was evaluated by the LIVE/DEAD viability assay. Representative fluorescent microscopic images from four independent experiments are shown. The graph depicts the percentages of dead cells. n = 4 experiments. Data are shown as mean ± SEM. ***p < 0.001 by a two-way ANOVA followed by the Bonferroni test. Scale bar: 20 μm. (**B**) Apoptosis was evaluated by immunocytochemical staining of cleaved caspase-3 (red), βIII tubulin (green) and DAPI staining (blue). Representative fluorescent microscopic images from four independent experiments are shown. The graph depicts the percentages of cleaved caspase-3-positive cells. n = 4 experiments. Data are shown as mean ± SEM. ***p < 0.001 by a two-way ANOVA followed by the Bonferroni test. Scale bar: 20 μm. (**C**) Apoptosis was evaluated by immunocytochemical staining of cleaved caspase-3 (red) and GFP (green) using primary hippocampal neurons transfected with vector, ATF6β cDNA or ATF6α cDNA together with GFP cDNA, followed by Tm treatment for 24 h. Representative fluorescent microscopic images are shown. Arrows indicate caspase-3-positive and GFP-positive cells. The graph depicts the percentages of cleaved caspase-3-positive cells out of GFP-positive cells. n = 400 cells per condition from two independent experiments. Data are shown as mean ± SEM. **p < 0.01, ***p < 0.001 by a two-way ANOVA followed by the Bonferroni test. Scale bar: 10 μm. Note that transfection of ATF6β cDNA, but not ATF6α cDNA, rescued $Atf6b^{-/-}$ neurons.
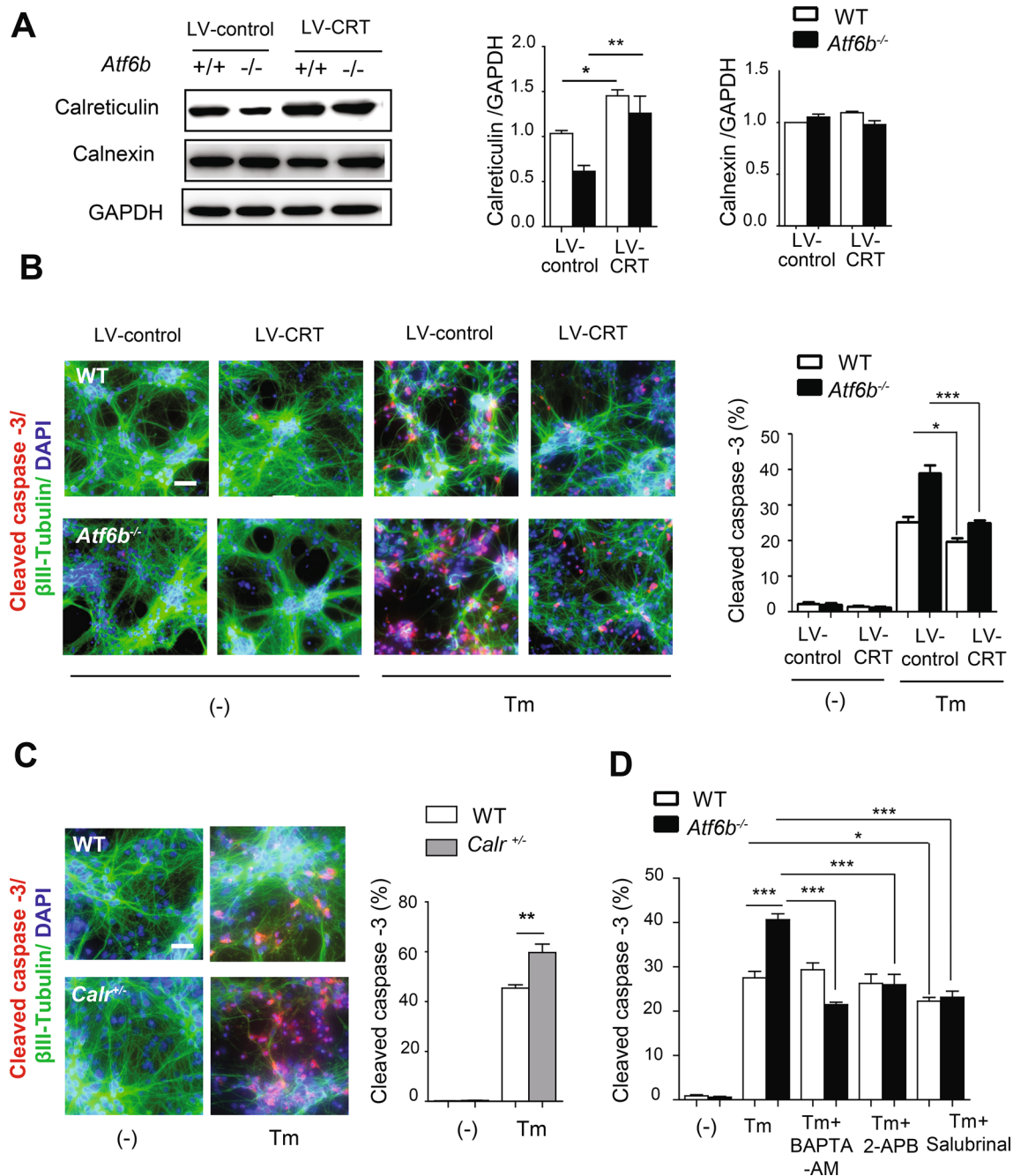
Figure 5. Protection of the primary hippocampal neurons by CRT or by treatment with Ca^{2+}/ER stress-modulating compounds. (**A,B**) WT and $Atf6b^{-/-}$ hippocampal neurons were infected with a control or CRT-expressing lentiviral vector, and the expression levels of CRT and calnexin were measured by western blotting (**A**). n = 3 experiments. Data are shown as mean ± SEM. *p < 0.05, **p < 0.01 by a two-way ANOVA followed by the Bonferroni tests. Cells were then treated with Tm (1 μg/ml) for 24 h, and cell death was evaluated by immunocytochemical staining for cleaved caspase-3 (**B**). Scale bar: 20 μm. n = 3 experiments. Data are shown as mean ± SEM. *p < 0.05, ***p < 0.001 by a two-way ANOVA followed by the Bonferroni test. (**C**) WT and $Calr^{+/-}$ primary hippocampal neurons were treated with Tm (1 μg/ml) for 24 h, and cell death was evaluated by immunocytochemical staining for cleaved caspase-3. n = 3 experiments. Scale bar: 20 μm. Data are shown as mean ± SEM. **p < 0.01 by a two-way ANOVA followed by the Bonferroni tests. (**D**) WT and $Atf6b^{-/-}$ hippocampal neurons were treated with Tm (1 μg/ml) together with BAPTA-AM (5 μM), 2-APB (2 μM) or salubrinal (5 μM). Cell death was evaluated by immunocytochemical staining for cleaved caspase-3. n = 3 experiments. Typical images are shown in Fig. S5. Data are shown as mean ± SEM. *p < 0.05, **p < 0.01, ***p < 0.001 by a two-way ANOVA followed by the Bonferroni test.
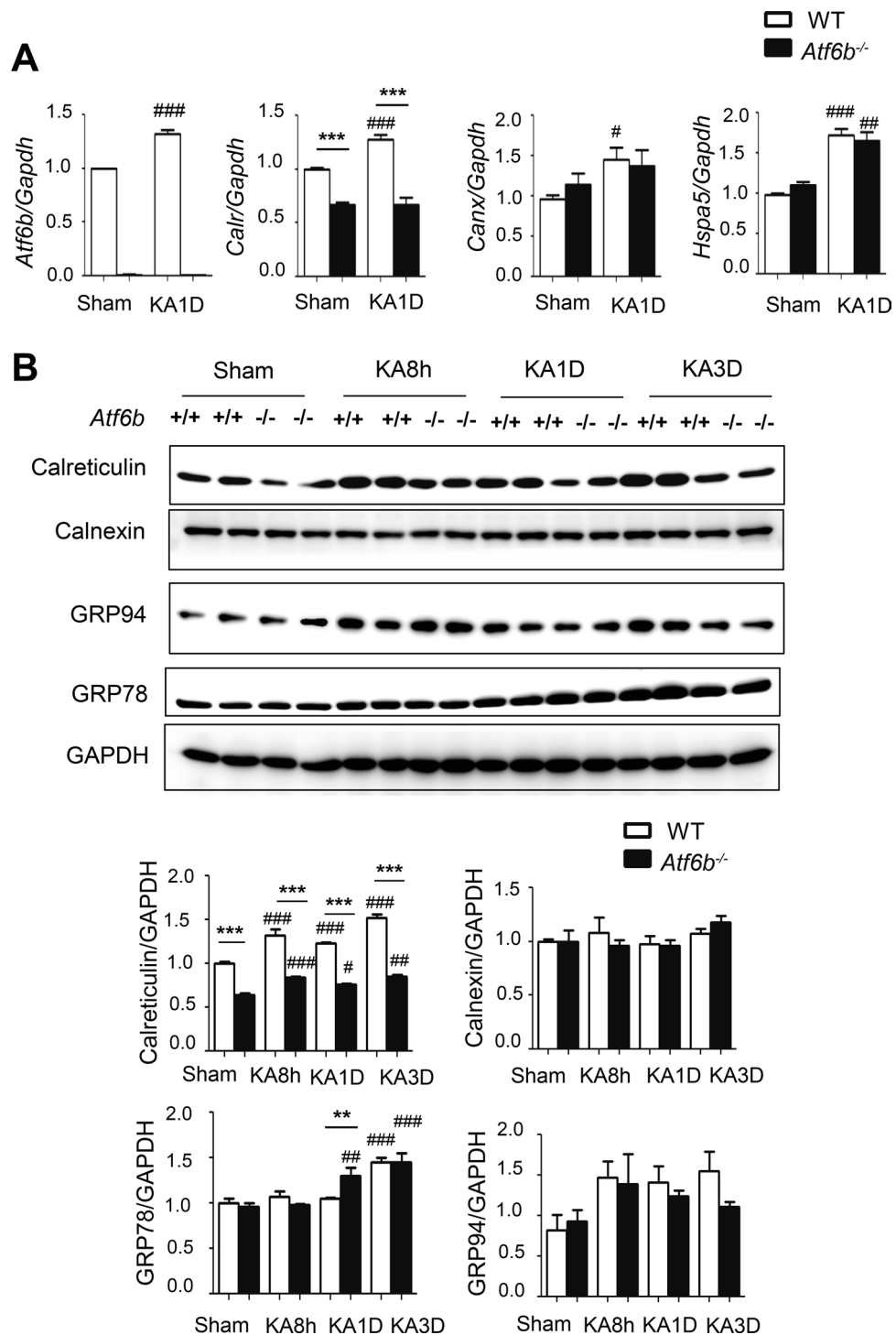
Figure 6. Expression of molecular chaperones in the ER in KA-injected mice. (**A**) Total RNA was isolated from the CA3 region of hippocampi from KA-injected WT and *Atf6b*^{−/−} mice and qRT-PCR was performed. n = 4 mice. Data are shown as mean ± SEM. ***p < 0.001 between two genotypes and #p < 0.05, ##p < 0.01, ###p < 0.001 compared to normal conditions by a two-way ANOVA followed by the Bonferroni test. (**B**) Protein samples were extracted from the CA3 region of hippocampi from KA-injected WT and *Atf6b*^{−/−} mice and subjected to western blotting using antibodies against CRT, calnexin, GRP94 and GRP78. n = 4–5 mice. Data are shown as mean ± SEM. **p < 0.001, ***p < 0.001 between two genotypes and #p < 0.05, ##p < 0.01, ###p < 0.001 compared to normal conditions by a two-way ANOVA followed by the Bonferroni test.
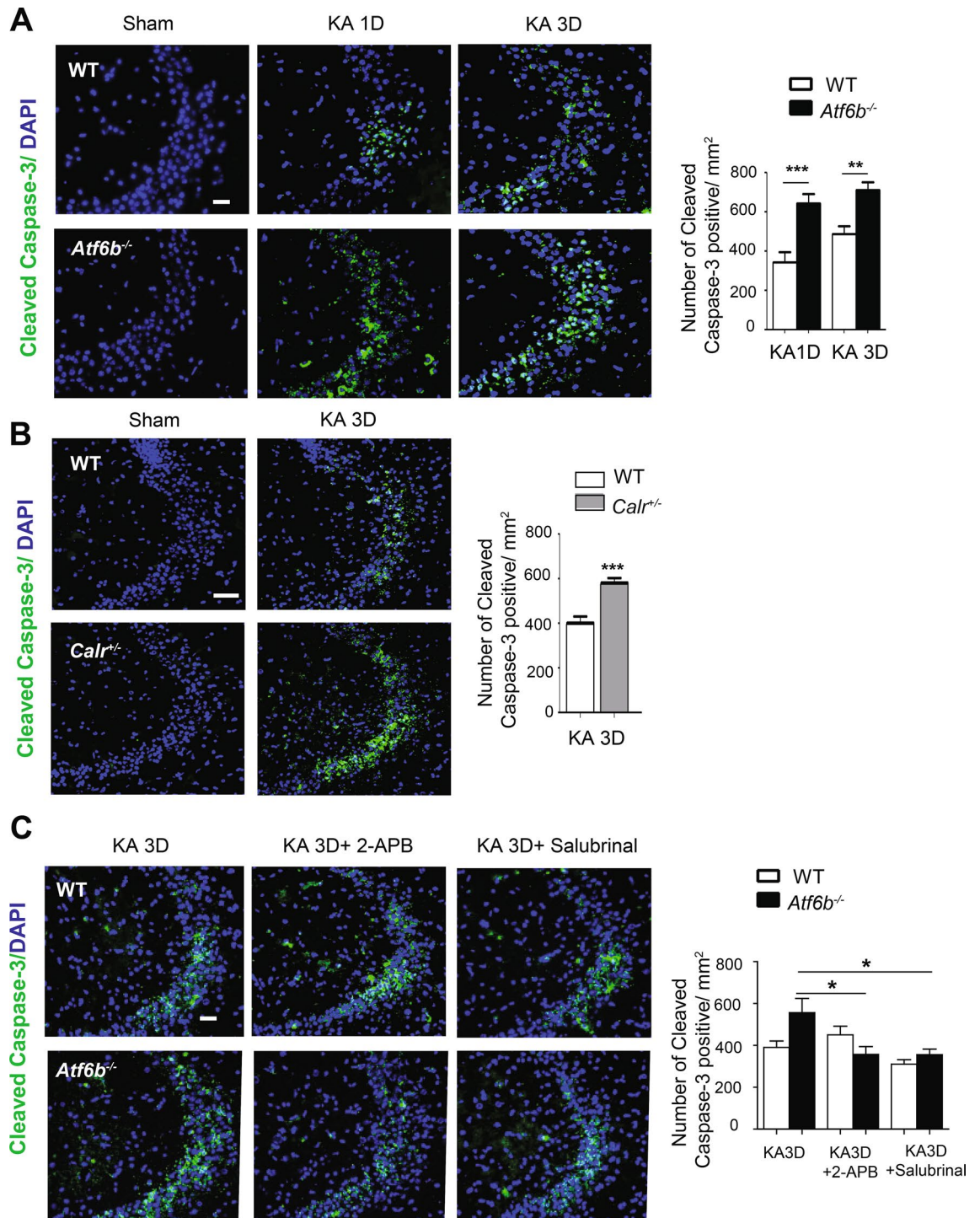
Figure 7. Neuroprotection by ATF6β and CRT through Ca^{2+} regulation in KA-injected mice. (**A,B**) Brain sections including the CA3 area of the hippocampus from WT and $Atf6b^{-/-}$ mice (**A**) (n = 6–7 mice) or WT and $Calr^{+/-}$ mice (**B**) (n = 6 mice) were subjected to immunohistochemical staining for cleaved caspase-3. The right graphs depict the number of cleaved caspase-3-positive CA3 neurons. Data are shown as mean ± SEM. **p < 0.01, ***p < 0.001 by a two-way ANOVA followed by the Bonferroni test in (**A**) and by the Mann–Whitney U test in (**B**). Scale bar: 50 μm. (**C**) Brain sections including the CA3 area of the hippocampus obtained from WT and $Atf6b^{-/-}$ mice at 3 days after injection with KA, KA plus 2-APB and KA plus salubrinal were subjected to immunohistochemical staining for cleaved caspase-3. The right graph depicts the number of cleaved caspase-3-positive cells. n = 6 mice. Data are shown as mean ± SEM. *p < 0.05 by a two-way ANOVA followed by the Bonferroni test.

and *Bdnf* was induced in both genotypes after KA-injection, but was higher in *Atf6b*$^{-/-}$ mice, suggesting that hyperactivity is involved in the enhanced level of neuronal death in the *Atf6b*$^{-/-}$ hippocampus. The effects of the Ca^{2+}-modulating reagent 2-APB and ER stress inhibitor salubrinal were next analyzed. They did not cause neuronal death at the doses used in this study (Fig. S9C). Immunohistochemical analysis revealed that both reagents significantly improved neuronal survival in the *Atf6b*$^{-/-}$ hippocampus after KA injection (Fig. 7C, Supplementary Fig. S9D), suggesting that temporal dysregulation of Ca^{2+} homeostasis in *Atf6b*$^{-/-}$ neurons enhances ER stress, leading to increased ER stress-induced neuronal death.

Finally, the Morris water maze test was performed to analyze the effect of ATF6β deletion on the spatial memory, which is typically associated with the hippocampal function. No significant differences were observed between WT and *Atf6b*$^{-/-}$ mice in either escape latency (Fig. S10B) or the time spent in the approach (Fig. S10C) and evacuation zone (Fig. S10D), suggesting the maintenance of hippocampal function in *Atf6b*$^{-/-}$ mice in normal condition.

Discussion

The major findings of the current study are that ATF6β specifically regulates CRT expression in the CNS and that the ATF6β-CRT axis plays an important role for the survival of hippocampal neurons upon exposure to ER stress and excitotoxicity.

CRT is a Ca^{2+}-binding molecular chaperone in the ER that functions in diverse cellular processes such as Ca^{2+} homeostasis, protein folding, gene expression, adhesion, and cell death[19,25]. It is also important for organogenesis especially in the heart, brain, and ventral body wall[26]. Deficiency of CRT leads to defects in myofibrillogenesis and thinner ventricular walls in the heart[27]. Interestingly, overexpression of CRT in the heart also causes severe phenotypes such as arrhythmias and sudden heart block following birth[28]. Therefore, the transcription of CRT in the heart is strictly controlled by several transcriptional factors such as Nkx2.5, COUP-TF1, GATA6 and Evi-1[29]. CRT is also highly expressed in the developing brain and retina, and its deficiency leads to a defect in closure of neural tubes[26]. Although it is unclear whether overexpression of CRT is toxic in the CNS, it is possible that the similar strict regulation of CRT expression is required and that ATF6β is utilized in addition to ATF6α for this purpose.

Our results suggest a novel role for ATF6β in the regulation of molecular chaperones in the ER. CRT expression was constitutively reduced to ~ 50% in the CNS of *Atf6b*$^{-/-}$ mice at both mRNA and protein levels. This was in contrast with other molecular chaperones in the ER. Expressions of calnexin, GRP94, and GRP78 were only temporally reduced in the *Atf6b*$^{-/-}$ neurons under ER stress condition at the mRNA level (Fig. 3A), but not at the protein level (Fig. 3B). These observations may raise a scenario that, in the CNS, the expression of molecular chaperones in the ER is generally governed by ATF6α as previously described[7] and that ATF6β functions as a booster if their levels are not high enough. However, neurons may require a high level of CRT expression even under normal conditions as described in Table S2, meaning that ATF6β are required to enhance CRT expression. This may increase the dependency of the CRT promoter on ATF6β, which would explain why CRT expression was not reduced in the brain of *Atf6a*$^{-/-}$ mice (Fig. S3A). Alternatively, it may be possible that some regulatory molecules suppress the transcriptional activity of ATF6β to maintain ATF6α-dependency for molecular chaperones in the ER except CRT. Further studies, especially those to find binding partners of ATF6β, are required to clarify the molecular basis how this unique system is regulated.

The current study also suggest a neuroprotective role of ATF6β which is associated with CRT-mediated Ca^{2+} homeostasis. *Atf6b* deficiency reduced CRT expression (Fig. 3A,B), decreased/increased basal Ca^{2+} levels in the ER/cytosol (Fig. 3C), and enhanced ER stress-induced death of cultured hippocampal neurons (Fig. 4A,B) and Neuro 2a cells (Fig. S6). Overexpression of ATF6β and CRT, but not ATF6α, rescued *Atf6b*$^{-/-}$ hippocampal neurons against ER stress-induced death (Figs. 4C, 5A,B). The lack of rescuing effect by ATF6α may be due to the fact that this molecule enhances the expression of different genes including cell death-related molecule CHOP in addition to molecular chaperons in the ER[30]. Consistent with the close relationship between ATF6β and Ca^{2+} homeostasis, treatment with Ca^{2+}-modulating reagents such as BAPTA-AM and 2-APB and with an ER stress inhibitor salubrinal restored the survival of *Atf6b*$^{-/-}$ neuronal cells under ER stress (Fig. 5D, Supplementary Fig. S7A,C). Our results in vivo also demonstrated that reduced level of CRT in *Atf6b*$^{-/-}$ neurons enhanced Ca^{2+}-mediated hyperactivity and ER stress after KA injection (Fig. 7, Supplementary Fig. S9). To our knowledge, this is the first report to demonstrate the impaired Ca^{2+} homeostasis and susceptibility of *Atf6b*$^{-/-}$ and *Calr*$^{+/-}$ hippocampal neurons to ER stress and excitotoxicity (Fig. 7B). Because *Atf6a* deficiency also enhances Kainate-induced neuronal death in vivo[10], it is intriguing to study the expression of CRT and other Ca^{2+} regulating molecules in *Atf6a*$^{-/-}$ brains after KA injection.

Accumulating evidence suggests that a reduced level of CRT is associated with the pathologies of neurodegenerative diseases such as amyotrophic lateral sclerosis (ALS)[23,31] and Alzheimer's disease (AD)[22,32]. In a mutant superoxide dismutase (mSOD1) model of ALS, activation of the Fas/nitric oxide (NO) pathway reduced CRT expression in motoneurons, which further activated Fas/NO signaling on one hand and enhanced ER stress and neuronal death on the other hand[23]. Consequently, the level of CRT was drastically decreased in 50% of fast fatigable motoneurons[31]. Although it is unclear whether ATF6β is involved in the Fas/NO-mediated reduction of the CRT expression, it will be intriguing to analyze the expression profile of ATF6β in these models.

Consistent with the observations in ALS, the level of CRT was reduced in the brains[22] and sera[32] of AD patients, raising the possibility that CRT is a good biomarker of AD[32]. However, it was also reported that a portion of CRT was located on the cell surface membrane, and acted as a receptor for C1q, the recognition subunit of the first component of complement. The C1q-CRT complex then induced oxidative neurotoxicity[33]; therefore, CRT may also have a pathological role in AD. Further analysis is required to elucidate the precise role of CRT and involvement of ATF6β in AD.

Although the function of ATF6β has been considered to be very limited or redundant compared with that of ATF6α, our results emphasize the critical and beneficial roles of ATF6β in the CNS. A recent study also demonstrated that ATF6β was functional in the heart, especially during the pressure overload-induced cardiac hypertrophic response[16]. The role of ATF6β may be determined by the need for specific molecular chaperones in the ER such as CRT, which may differ between tissues. Further studies dissecting the cell- and tissue-specific roles of ATF6β will help to elucidate the function of the UPR in pathophysiological conditions.

Materials and methods

Animals.   All animal experiments including behavioral study were approved by the Animal Care and Use Committee of Kanazawa University (Approval No. AP-184013) and by the institutional review committee of Kanazawa Medical University (Approval No. 2018-21). They were conducted in accordance with the Fundamental Guidelines for Proper Conduct of Animal Experiment and Related Activities in Academic Research Institutions under the jurisdiction of the Ministry of Education, Culture, Sports, Science and Technology, as well as in compliance with the ARRIVE guidelines. $Atf6a^{+/-}$ and $Atf6b^{+/-}$ mice were generated as previously described[7], and backcrossed with the C57BL/6 strain for more than eight times at the Institute of Laboratory Animals, Graduate School of Medicine, Kyoto University. $Atf6a^{+/-}$ and $Atf6b^{+/-}$ mice were intercrossed to obtain wild-type (WT), $Atf6a^{-/-}$, and $Atf6b^{-/-}$ mice. These lines were maintained by mating mice of the same genotype at the Institute for Experimental Animals, Advanced Science Research Center, Kanazawa University. Mice used in behavioral study were propagated by mating $Atf6b^{+/-}$ mice, thereby producing $Atf6b^{+/+}$, $Atf6b^{+/-}$, and $Atf6b^{-/-}$ offspring. $Atf6b^{+/+}$ mice were used as WT controls. $Calr^{+/-}$ mice were generated as previously described[34], and provided by the RIKEN BioResource Research Center (Tsukuba, Ibaraki, Japan). $Calr^{+/-}$ mice were maintained by mating mice with WT mice in the C57BL/6 background. WT, $Atf6a^{-/-}$, $Atf6b^{-/-}$, and $Calr^{+/-}$ mice (age, 10–12 weeks; weight, 25–30 g) were used for experiments expect behavioral study. In behavioral study, age-matched WT and $Atf6b^{-/-}$ mice (18–21 weeks) were used.

Kainate (KA) injection in mice.   To develop a KA injection model, male mice were anesthetized, and saline or KA (0.2 μg/μl, 0.5 μl in total; Sigma, St Louis, MO, USA) was injected unilaterally into the hippocampus (from Bregma: dorso-ventral, −2.0; medio-lateral, −2.4; anterior–posterior, −1.8), as previously described[10]. In some cases, 2-APB (12 μM, 0.5 μl in total; FUJIFILM Wako Pure Chemical Co., Osaka, Osaka, Japan) or salubrinal (1 mg/kg; Cayman Chemical, Ann Arbor, MI, USA) was co-injected with KA into the hippocampus, or intraperitoneally injected 30 min before KA administration, as previously described[2,35,36]. Mice were sacrificed at the indicated timepoints after KA injection, and brain samples were prepared for histological and biochemical analysis.

Morris water maze test.   The Morris water maze test was conducted as described previously[37]. A plastic cylindrical tank (120 cm φ) surrounded by a wall of 45 cm high and filled with opaque water (25 °C) was used. A transparent plastic platform (10 cm φ) was hidden below the water surface. Four differently-shaped and -colored objects were placed above the edge of the tank as geographical external cues. On each of 5 consecutive days, mice were given 4 sessions of swim. For each session, the mice were released from a starting point pseudo-randomly chosen from the 4 positions, and the time spent to reach the platform (escape latency) was measured. If mice were not able to reach the platform within 60 s, they were placed on the platform by the experimenter and allowed to stay there for 20 s. The average of the time spent over the 4 sessions yielded the latency score for a particular day for an individual mouse. The day-by-day averages were then calculated for each group. After the last goal-seeking session on the last test day, the platform was removed to perform the probe test. The mice were placed into the water from the edge of the pool located opposite to the former platform position, and allowed to swim for 60 s. The swimming trajectory was digital video-recorded and analyzed offline (SMART, Panlab Harvard Apparatus, Barcelona, Spain). The time spent in the approach and evacuation zone were calculated and expressed as percentage over the total time of 60 s.

Cell cultures.   Primary hippocampal and cortical neurons were isolated from embryonic day 17.5 (E17.5) WT, $Atf6b^{-/-}$, $Calr^{+/-}$ and WT mice, as previously described, with minor modifications[38]. Briefly, hippocampi and cerebral cortices were harvested from prenatal mice, and digested using neuron dissociation solution (FUJIFILM Wako Pure Chemical Co.). After isolation, neurons were plated into 24-well culture plates precoated with poly-L-lysine (10 μg/ml; Sigma) at a density of 8×10^5 cell/well, and cultured in Neurobasal Medium (Life Technologies, Carlsbad, CA, USA) supplemented with 2% B-27 serum free supplement (Life Technologies), 0.4 mM L-glutamine (Sigma), 5% fetal bovine serum (FBS)(Sigma), 100 U/ml penicillin and 100 μg/ml streptomycin (Nacalai Tesque, Kyoto, Kyoto, Japan). After 3 days, neurons were used for experiments. Hippocampal neurons were treated with the ER stressors Tg (300 nM; Sigma), DTT (1 mM; Nacalai Tesque) and Tm (1 μg/ml; FUJIFILM Wako Pure Chemical Co.). In some cases, they were treated with BAPTA-AM (5 μM; Dojindo Molecular and Technologies Inc., Mashiki-machi, Kumamoto, Japan), 2-APB (2 μM) or salubrinal (5 μM) in addition to Tm for the indicated durations.

Astrocytes were isolated from the cerebral cortex of postnatal day 1–3 WT mice, as previously described[39], and cultured in Dulbecco's Modified Eagle Medium (DMEM) supplemented with 10% FBS and penicillin/streptomycin. Cells were used for experiments after achieving full confluency.

MEFs were isolated from the skin of E15.5 WT and $Atf6b^{-/-}$ mice, as previously described[7], and were cultured in DMEM supplemented with 20% FBS and penicillin/streptomycin. Cells were used for experiments after achieving full confluency.

Neuro 2a cells were plated at a density of 5×10^4 cells/well in 24- or 12-well culture plates, and cultured in DMEM supplemented with 10% FBS and penicillin/streptomycin. Cells were used for experiments after achieving 70% of confluency.

Preparation and transfection of plasmids. Plasmids expressing full length mouse ATF6α and ATF6β were constructed by inserting ATF6α and ATF6β cDNAs into the pCDF1-MCS2-EF1-Puro expression vector (System Biosciences, Palo Alto, CA, USA). Plasmids expressing the active and dominant-negative forms of human ATF6β, ATF6β(392) and ATF6β(392)ΔAD, respectively, were constructed in pcDNA3.1(+), as previously described[14]. pcDNA3.1(+) GFP was obtained from Invitrogen/Thermo Fisher Scientific (Waltham, MA, USA). CAT plasmids containing the mouse CRT promoter (pCC1, pCC3, and pCC5) were provided by Dr. Marek Michalak (University of Alberta)[17]. Both of pCC1 and pCC3, but not pCC5, contain ERSE, a consensus of CCAATN$_9$CCACG[18] (Fig. 3A). Luciferase plasmids containing huCRT(wt) and huCRT(mut), with the two ERSEs mutated in the latter, and a plasmid containing the WT human GRP78 promoter (huGRP78) were constructed as previously described[18]. The pRL-SV40 plasmid was obtained from Promega (Madison, WI, USA). Plasmids for Ca^{2+} imaging such as pCMV G-CEPIA1er, pGP-CMV-GCaMP6f and pCMV CEPIA2mt were obtained from Addgene (Watertown, MA, USA). Cells were transfected with each plasmid for 5 h using Lipofectamine 2000 (Life Technologies) and further incubated for 24–48 h. In our model, transfection efficiency was approximately 5% in primary neurons.

Preparation and infection of lentivirus vectors. The lentivirus vector expressing full-length mouse CRT under the control of the human eukaryotic translation elongation factor 1 α1 promoter and the lentivirus vector alone was purchased from VectorBuilder (Chicago, IL, USA). Viral stocks had titers of ~ 10^9 plaque-forming units/ml. Hippocampal neurons were infected with the CRT-expressing (LV-CRT) or control (LV-control) lentivirus vector at a multiplicity of infection 10 for 16 h and further incubated for 48–72 h.

Preparation and transfection of ATF6β-targeting siRNAs. ATF6β-specific siRNAs, namely, ATF6β-siRNA1 (SASI_Mm01_00110468) and ATF6β-siRNA2 (SASI_Mm01_00110470), and control-siRNA were obtained from Sigma. Neuro2a cells were transfected with each siRNA for 5 h using Lipofectamine RNAiMAX (Life Technologies) and further incubated for 24–48 h.

qRT-PCR. Total RNA was extracted from the indicated mouse tissues and cultured cells using RNeasy Lipid Tissue Mini Kit (Qiagen, Valencia, CA, USA). Reverse transcription reactions containing 1 µg of total RNA were performed using PrimeScript (Takara, Otsu, Shiga, Japan). Individual cDNAs were amplified with THUNDERBIRD SYBR qPCR Mix (TOYOBO CO, LTD, Osaka, Osaka, Japan) using specific primers for *Atf6b*, *Atf6a*, *Calr*, *Canx*, *Hspa5*, *Hsp90b1*, *Fos*, *Fosb*, *Bdnf* and *Gapdh*. The primers are listed in Table S3. The comparative Ct method was used for data analyses with MxPro 4.10 (Agilent Technologies, Santa Clara, CA, USA). Values for each gene were normalized against the *Gapdh* expression level.

Western blotting. Samples from the indicated mouse tissues and cultured cells were solubilized in RIPA buffer, which contained 10 mM Tris (pH 7.6), 1 mM EDTA, 150 mM NaCl, 1% NP-40, 0.1% SDS, 0.2% sodium deoxycholate, 1 mM PMSF, 1 µg/ml aprotinin, 10 mM NaF, and 1 mM Na$_3$VO$_4$. To detect endogenous ATF6β protein in primary hippocampal neurons, RIPA buffer without sodium deoxycholate was used. Membranes were incubated with 3% bovine serum albumin for 1 h and then with the primary antibodies for overnight at 4 ℃. The primary antibodies included those against ATF6β (853,202; BioLegend, San Diego, CA, USA; 1:500), CRT (SPA-600; Enzo Life Sciences Inc., Farmingdale, NY, USA; 1:2000 and 10,292–1-AP; Proteintech, Rosemont, IL, USA; 1:1000), calnexin (SPA-865; Enzo Life Sciences Inc.; 1:1000), KDEL (PM-059; Medical & Biological Laboratories, Nagoya, Aichi, Japan; 1:1000), and GAPDH (016-25523; FUJIFILM Wako Pure Chemical Co.; 1:2000). Sites of primary antibody binding were determined using an enhanced chemiluminescence system (GE Healthcare, Pittsburgh, PA, USA). Horseradish peroxidase (HRP)-conjugated secondary antibodies (Santa Cruz Biotechnology, Dallas, TX, USA) were used to detect immunoglobulins from mouse or rabbit. The intensity of each band was quantified by using Image J software (version 1.50i, Wayne Rasband, National Institutes of Health, Bethesda, MD, USA, https://imagej.nih.gov/ij/). Uncropped gel files with molecular weight markers of western blotting are shown in Figs. S10 and S11.

Histology and immunohistochemistry. At the indicated timepoints after KA injection, mice (WT, *Atf6b*$^{-/-}$, and *Calr*$^{+/-}$) were deeply anesthetized with isoflurane and transcardially perfused with phosphate-buffered saline (PBS) followed by 4% paraformaldehyde prepared in 0.1 M phosphate buffer (pH 7.4). Brains were harvested, post-fixed with 4% paraformaldehyde for 8 h, and cryoprotected in 30% sucrose for at least 24 h. Cortical Sects. (10 µm-thick coronal sections containing the hippocampus (between Bregma − 1.5 and − 2.1 mm)) were cut on a cryostat (Leica Biosystems, Wetzler, Germany). Sections were processed for Nissl staining (Cresyl violet staining) or immunohistochemistry with antibodies against cleaved caspase-3 (Asp175; Cell Signaling Technology, Inc. Danvers, MA, USA; 1:500) and c-Fos (PC05; Merck; 1:200). Nuclei were visualized with 4′,6-diamidino-2-phenylindole (DAPI; Sigma). Anti-rabbit and anti-mouse Alexa Fluor 488-conjugated (Life Technologies; 1:200) and Cy3-conjugated (Jackson ImmunoResearch Laboratories, Inc., West Grove, PA, USA; 1:200) secondary antibodies were used to visualize immunolabeling. Imaging was performed using a laser scanning confocal microscope (Eclipse TE200U; Nikon, Tokyo, Japan) and Nikon EZ-C1 software or using a light and fluorescence microscope (BZ-X700; KEYENCE, Osaka, Japan).

In situ hybridization-immunohistochemistry. In situ hybridization was performed as previously described[40]. In brief, a ~ 600 bp mouse ATF6β cDNA fragment was PCR-amplified using 5′-AACAGGAAGGTT GTCTGCATCAT-3′ and 5′-GTATCCTCCCTCCGGTCAAT-3′ primers and inserted into the pGEM-T vector (Promega). The plasmid was linearized using EcoRV and ApaI to synthesize the antisense and sense probe, respectively. Brains were removed from mice after perfusion with PBS and immediately placed at − 80 ℃. Serial 14 μm-thick coronal sections were obtained using a cryostat and hybridized with a digoxigenin-labeled ATF6β RNA probe. After development and thorough washing with PBS, brain sections were subjected to immunohisto-chemistry using a mouse anti-NeuN antibody (MAB377; Merck, Kenilworth, NJ, USA; 1:500) followed by incu-bation with an anti-mouse IgG antibody (Vector Laboratories, Inc., Burlingame, CA, USA). The sections were developed in peroxidase substrate solution (ImmPACT DAB, Vector Laboratories, Inc.). Imaging was performed using a light and fluorescence microscope (BZ-X700, KEYENCE).

RNA-sequencing. Total RNA purified from hippocampi of WT and *Atf6b⁻/⁻* mice (n = 2 per group) was used to prepare RNA libraries using a TruSeq Stranded mRNA Sample Preparation Kit (Illumina, Inc., San Diego, CA, USA), with polyA selection for ribosomal RNA depletion. The RNA libraries were generated from 500 ng of total hippocampal RNA and sequenced on an Illumina HiSeq 2000 to obtain paired-end 101 bp reads for each sample.

RNA-sequencing reads were mapped to the Mouse genome (GRCm.38.p6/mm10) using STAR v2.7.0f[41]. Aligned reads were counted and assigned to genes using Ensembl release 99 gene annotation[42]. Gene expression levels were quantified using Cufflinks v2.2.1[43], and denoted by fragments per kilobase of exon per million reads mapped (FPKM) values, which were normalized by the number of RNA fragments mapped to the reference genome and the total length of all exons in the respective transcripts. Differentially expressed genes between WT and *Atf6b⁻/⁻* hippocampi were identified by Cuffdiff, which is part of the Cufflinks toolkit. Two replicates per group were combined as the input of Cuffdiff, and q- and p-values were reported to show the significance of differentially expressed genes. The raw reads are available in the DNA Data Bank of Japan (DDBJ) with DDBJ Sequence Read Archive (DRA) accession number, DRA011345.

Ca²⁺ measurement in the intracellular organelles and in the cytosol. Ca²⁺ levels in the ER, cyto-sol and mitochondria of hippocampal neurons were measured using G-CEPIA1er, GCaMP6f and CEPIA2mt, respectively. Forty-eight hours after transfection, Ca²⁺ imaging was performed using a light and fluorescence microscope (BZ-X700, KEYENCE) under normal and ER stress conditions. The intensity of the fluorescence in each cell was measured using ImageJ software for 60–250 cells neurons in each condition.

Immunocytochemistry. Cultured hippocampal neurons and Neuro 2a cells were fixed in 4% paraform-aldehyde for 15 min at room temperature, and permeabilized in 0.3% Trinton-X100 for 10 min. Primary anti-bodies against GFP (MBL598; Merck; 1:500), Myc (sc-40; Santa Cruz Biotechnology; 1:200), cleaved caspase-3 (Asp175, Cell Signaling Technology, Inc; 1:800) andβIII tubulin (MAB1637; Merck; 1:500) were used. Nuclei were visualized with DAPI (Sigma). Imaging was performed using a light and fluorescence microscope (BZ-X700, KEYENCE).

LIVE/DEAD viability assay. Living and dead neurons and Neuro 2a cells were evaluated using a LIVE/DEAD Viability Assay kit (Life Technologies). In brief, cells were washed in PBS and incubated with calcein-AM (1 μM), EthD-1 (2 μM) and Hoechst 33,342 (1 μg/ml, Dojindo Molecular and Technologies Inc.) in regular medium. Imaging was performed using a fluorescence microscope (BZ-X700, KEYENCE).

Reporter assay. *Luciferase assay.* At 48 h after transfection, cells were lysed in 100 μl of Passive Lysis Buffer (Promega). Firefly luciferase and Renilla luciferase activities were measured using the Dual-Luciferase Reporter Assay System (Promega) and analyzed as previously describe[18].

CAT ELISA. At 48 h after transfection, cells were lysed in 125 μl of lysis buffer provided with a CAT ELISA kit (Sigma). CAT expression and Renilla luciferase activities were measured and the ratio was calculated.

Image quantification. For the LIVE/DEAD viability assay and immunocytochemistry, four images per well were acquired and the numbers of EthD-1-positive cells/Hoechst 33342-positive cells and cleaved caspase-3-positive cells/DAPI-positive total cells were counted using ImageJ software, respectively. For Nissl staining, three brain sections containing the hippocampal CA3 area close to the KA injection site were selected per mouse and the number of Nissl-positive neurons was counted using ImageJ software. For immunohistochemistry, two brain sections with the highest numbers of cleaved caspase-3-positive cells and c-Fos-positive cells were selected per mouse, and the numbers of these cells were counted using ImageJ software.

Statistical analyses. Statistical analyses were performed using the Mann–Whitney U test or a one-way or two-way analysis of variance (ANOVA) followed by the Tukey/Bonferroni test. GraphPad Prism software 5.0 was used for statistical analyses. A p-value less than 0.05 was considered statistically significant.

References

1. Bukau, B., Weissman, J. & Horwich, A. Molecular chaperones and protein quality control. *Cell* **125**, 443–451. https://doi.org/10.1016/j.cell.2006.04.014 (2006).
2. Sokka, A. L. *et al.* Endoplasmic reticulum stress inhibition protects against excitotoxic neuronal injury in the rat brain. *J. Neurosci.* **27**, 901–908. https://doi.org/10.1523/jneurosci.4289-06.2007 (2007).
3. Sprenkle, N. T., Sims, S. G., Sanchez, C. L. & Meares, G. P. Endoplasmic reticulum stress and inflammation in the central nervous system. *Mol. Neurodegener.* **12**, 42. https://doi.org/10.1186/s13024-017-0183-y (2017).
4. Thiebaut, A. M., Hedou, E., Marciniak, S. J., Vivien, D. & Roussel, B. D. Proteostasis during cerebral ischemia. *Front. Neurosci.* **13**, 637. https://doi.org/10.3389/fnins.2019.00637 (2019).
5. Mori, K. Signalling pathways in the unfolded protein response: Development from yeast to mammals. *J. Biochem.* **146**, 743–750. https://doi.org/10.1093/jb/mvp166 (2009).
6. Walter, P. & Ron, D. The unfolded protein response: From stress pathway to homeostatic regulation. *Science* **334**, 1081–1086. https://doi.org/10.1126/science.1209038 (2011).
7. Yamamoto, K. *et al.* Transcriptional induction of mammalian ER quality control proteins is mediated by single or combined action of ATF6alpha and XBP1. *Dev. Cell* **13**, 365–376. https://doi.org/10.1016/j.devcel.2007.07.018 (2007).
8. Ishikawa, T. *et al.* ATF6alpha/beta-mediated adjustment of ER chaperone levels is essential for development of the notochord in medaka fish. *Mol. Biol. Cell* **24**, 1387–1395. https://doi.org/10.1091/mbc.E12-11-0830 (2013).
9. Kitao, Y. *et al.* Expression of the endoplasmic reticulum molecular chaperone (ORP150) rescues hippocampal neurons from glutamate toxicity. *J. Clin. Investig.* **108**, 1439–1450. https://doi.org/10.1172/jci12978 (2001).
10. Kezuka, D. *et al.* Deletion of Atf6alpha enhances kainate-induced neuronal death in mice. *Neurochem. Int.* **92**, 67–74. https://doi.org/10.1016/j.neuint.2015.12.009 (2016).
11. Hashida, K. *et al.* ATF6alpha promotes astroglial activation and neuronal survival in a chronic mouse model of Parkinson's disease. *PLoS ONE* **7**, e47950. https://doi.org/10.1371/journal.pone.0047950 (2012).
12. Yoshikawa, A. *et al.* Deletion of Atf6alpha impairs astroglial activation and enhances neuronal death following brain ischemia in mice. *J. Neurochem.* **132**, 342–353. https://doi.org/10.1111/jnc.12981 (2015).
13. Ta, H. M. *et al.* Atf6alpha deficiency suppresses microglial activation and ameliorates pathology of experimental autoimmune encephalomyelitis. *J. Neurochem.* **139**, 1124–1137. https://doi.org/10.1111/jnc.13714 (2016).
14. Haze, K. *et al.* Identification of the G13 (cAMP-response-element-binding protein-related protein) gene product related to activating transcription factor 6 as a transcriptional activator of the mammalian unfolded protein response. *Biochem. J.* **355**, 19–28. https://doi.org/10.1042/0264-6021:3550019 (2001).
15. Lynch, J. M. *et al.* A thrombospondin-dependent pathway for a protective ER stress response. *Cell* **149**, 1257–1268. https://doi.org/10.1016/j.cell.2012.03.050 (2012).
16. Correll, R. N. *et al.* Overlapping and differential functions of ATF6alpha versus ATF6beta in the mouse heart. *Sci. Rep.* **9**, 2059. https://doi.org/10.1038/s41598-019-39515-5 (2019).
17. Waser, M., Mesaeli, N., Spencer, C. & Michalak, M. Regulation of calreticulin gene expression by calcium. *J. Cell Biol.* **138**, 547–557. https://doi.org/10.1083/jcb.138.3.547 (1997).
18. Yoshida, H., Haze, K., Yanagi, H., Yura, T. & Mori, K. Identification of the cis-acting endoplasmic reticulum stress response element responsible for transcriptional induction of mammalian glucose-regulated proteins. Involvement of basic leucine zipper transcription factors. *J. Biol. Chem.* **273**, 33741–33749. https://doi.org/10.1074/jbc.273.50.33741 (1998).
19. Michalak, M., Groenendyk, J., Szabo, E., Gold, L. I. & Opas, M. Calreticulin, a multi-process calcium-buffering chaperone of the endoplasmic reticulum. *Biochem. J.* **417**, 651–666. https://doi.org/10.1042/bj20081847 (2009).
20. Suzuki, J. *et al.* Imaging intraorganellar Ca2+ at subcellular resolution using CEPIA. *Nat. Commun.* **5**, 4153. https://doi.org/10.1038/ncomms5153 (2014).
21. Chen, T. W. *et al.* Ultrasensitive fluorescent proteins for imaging neuronal activity. *Nature* **499**, 295–300. https://doi.org/10.1038/nature12354 (2013).
22. Taguchi, J. *et al.* Different expression of calreticulin and immunoglobulin binding protein in Alzheimer's disease brain. *Acta Neuropathol.* **100**, 153–160. https://doi.org/10.1007/s004019900165 (2000).
23. Bernard-Marissal, N. *et al.* Reduced calreticulin levels link endoplasmic reticulum stress and Fas-triggered cell death in motoneurons vulnerable to ALS. *J. Neurosci.* **32**, 4901–4912. https://doi.org/10.1523/jneurosci.5431-11.2012 (2012).
24. Paschen, W., Hotop, S. & Aufenberg, C. Loading neurons with BAPTA-AM activates xbp1 processing indicative of induction of endoplasmic reticulum stress. *Cell Calcium* **33**, 83–89. https://doi.org/10.1016/s0143-4160(02)00195-1 (2003).
25. Wang, W. A., Groenendyk, J. & Michalak, M. Calreticulin signaling in health and disease. *Int. J. Biochem. Cell Biol.* **44**, 842–846. https://doi.org/10.1016/j.biocel.2012.02.009 (2012).
26. Rauch, F., Prud'homme, J., Arabian, A., Dedhar, S. & St-Arnaud, R. Heart, brain, and body wall defects in mice lacking calreticulin. *Exp. Cell Res.* **256**, 105–111. https://doi.org/10.1006/excr.2000.4818 (2000).
27. Mesaeli, N. *et al.* Calreticulin is essential for cardiac development. *J. Cell Biol.* **144**, 857–868. https://doi.org/10.1083/jcb.144.5.857 (1999).
28. Nakamura, K. *et al.* Complete heart block and sudden death in mice overexpressing calreticulin. *J. Clin. Investig.* **107**, 1245–1253. https://doi.org/10.1172/jci12412 (2001).
29. Qiu, Y. *et al.* Regulation of the calreticulin gene by GATA6 and Evi-1 transcription factors. *Biochemistry* **47**, 3697–3704. https://doi.org/10.1021/bi702524v (2008).
30. Yoshida, H. *et al.* ATF6 activated by proteolysis binds in the presence of NF-Y (CBF) directly to the cis-acting element responsible for the mammalian unfolded protein response. *Mol. Cell Biol.* **20**, 6755–6767. https://doi.org/10.1128/mcb.20.18.6755-6767.2000 (2000).
31. Bernard-Marissal, N., Sunyach, C., Marissal, T., Raoul, C. & Pettmann, B. Calreticulin levels determine onset of early muscle denervation by fast motoneurons of ALS model mice. *Neurobiol. Dis.* **73**, 130–136. https://doi.org/10.1016/j.nbd.2014.09.009 (2015).
32. Lin, Q., Cao, Y. & Gao, J. Serum calreticulin is a negative biomarker in patients with Alzheimer's disease. *Int. J. Mol. Sci.* **15**, 21740–21753. https://doi.org/10.3390/ijms151221740 (2014).
33. Luo, X., Weber, G. A., Zheng, J., Gendelman, H. E. & Ikezu, T. C1q-calreticulin induced oxidative neurotoxicity: Relevance for the neuropathogenesis of Alzheimer's disease. *J. Neuroimmunol.* **135**, 62–71. https://doi.org/10.1016/s0165-5728(02)00444-7 (2003).
34. Tokuhiro, K. *et al.* Calreticulin is required for development of the cumulus oocyte complex and female fertility. *Sci. Rep.* **5**, 14254. https://doi.org/10.1038/srep14254 (2015).
35. Kim, J. S. *et al.* Salubrinal, ER stress inhibitor, attenuates kainic acid-induced hippocampal cell death. *J. Neural Transm. (Vienna)* **121**, 1233–1243. https://doi.org/10.1007/s00702-014-1208-0 (2014).
36. Ikebara, J. M. *et al.* Functional role of intracellular calcium receptor inositol 1,4,5-trisphosphate type 1 in rat hippocampus after neonatal anoxia. *PLoS ONE* **12**, e0169861. https://doi.org/10.1371/journal.pone.0169861 (2017).

37. Wang, F. *et al.* Improvement of spatial learning by facilitating large-conductance calcium-activated potassium channel with transcranial magnetic stimulation in Alzheimer's disease model mice. *Neuropharmacology* **97**, 210–219. https://doi.org/10.1016/j.neuropharm.2015.05.027 (2015).
38. Kaech, S. & Banker, G. Culturing hippocampal neurons. *Nat. Protoc.* **1**, 2406–2415. https://doi.org/10.1038/nprot.2006.356 (2006).
39. McCarthy, K. D. & de Vellis, J. Preparation of separate astroglial and oligodendroglial cell cultures from rat cerebral tissue. *J. Cell Biol.* **85**, 890–902. https://doi.org/10.1083/jcb.85.3.890 (1980).
40. Hattori, T. *et al.* DISC1 (disrupted-in-schizophrenia-1) regulates differentiation of oligodendrocytes. *PLoS ONE* **9**, e88506. https://doi.org/10.1371/journal.pone.0088506 (2014).
41. Dobin, A. *et al.* STAR: Ultrafast universal RNA-seq aligner. *Bioinformatics* **29**, 15–21. https://doi.org/10.1093/bioinformatics/bts635 (2013).
42. Cunningham, F. *et al.* Ensembl 2019. *Nucleic Acids Res.* **47**, D745–D751. https://doi.org/10.1093/nar/gky1113 (2019).
43. Trapnell, C. *et al.* Differential analysis of gene regulation at transcript resolution with RNA-seq. *Nat. Biotechnol.* **31**, 46–53. https://doi.org/10.1038/nbt.2450 (2013).

Acknowledgements

Author contributions

D.T.N. and O.H. conceived and planned the experiments. D.T.N., T.M.L., J.R., T.Tamatani, T.K., K.H., S.T., M.M. and S.S. carried out the experiments except the behavioral experiment. T.Tanaka and N.K. performed the behavioral experiment and analyzed the data. T.H., M.T., H.I., A.T., S.O. and K.M. supervised the project. O.H. took the lead in writing the manuscript and prepared all figures. All authors provided critical feedback and helped shape the research, analysis and manuscript.

Competing interests

The authors declare no competing interests.

Additional information

Supplementary Information The online version contains supplementary material available at https://doi.org/10.1038/s41598-021-92529-w.

Correspondence and requests for materials should be addressed to O.H.

Reprints and permissions information is available at www.nature.com/reprints.

Publisher's note Springer Nature remains neutral with regard to jurisdictional claims in published maps and institutional affiliations.